Molecular Psychiatry (2017) 22, 1562–1575
www.nature.com/mp

OPEN

ORIGINAL ARTICLE

The transcription factor XBP1s restores hippocampal synaptic plasticity and memory by control of the Kalirin-7 pathway in Alzheimer model

M Cissé, E Duplan, T Lorivel, J Dunys, C Bauer, X Meckler, Y Gerakis, I Lauritzen and F Checler

Neuronal network dysfunction and cognitive decline constitute the most prominent features of Alzheimer's disease (AD), although mechanisms causing such impairments are yet to be determined. Here we report that virus-mediated delivery of the active spliced transcription factor X-Box binding protein 1s (XBP1s) in the hippocampus rescued spine density, synaptic plasticity and memory function in a mouse model of AD. XBP1s transcriptionally activated Kalirin-7 (Kal7), a protein that controls synaptic plasticity. In addition, we found reduced levels of Kal7 in primary neurons exposed to Aβ oligomers, transgenic mouse models and human AD brains. Short hairpin RNA-mediated knockdown of Kal7 altered synaptic plasticity and memory formation in naive mice. Further, reduction of endogenous Kal7 compromised the beneficial effects of XBP1s in Alzheimer's model. Hence, our findings reveal that XBP1s is neuroprotective through a mechanism that engages Kal7 pathway with therapeutic implications in AD pathology.

Molecular Psychiatry (2017) **22,** 1562–1575; doi:10.1038/mp.2016.152; published online 20 September 2016

INTRODUCTION

Spine development and plasticity are essential for normal cognitive function and underlie processes such as learning and memory. Abnormalities in spine formation and morphology are associated with numerous neurological and intellectual disorders, including Alzheimer's disease (AD).[1–6] AD is characterized histologically by intracellular neurofibrillary tangles and extracellular Aβ deposits in specific regions of the brain.[7] Loss of synapses in the hippocampus is a hallmark of AD[8] and acute Aβ exposure to neuronal cultures or slices reduces spine density and alters neuronal plasticity,[9–11] most likely by affecting proteins that regulate spinogenesis. Loss of dendritic spines directly correlates with the loss of synaptic function and deficits in memory.[12,13] Therefore, pharmacological strategies aimed at preserving the integrity of spines by targeting proteins that functionally regulate these neuronal structures could be beneficial in AD pathology. In this perspective, X-Box binding protein 1s (XBP1s), a sensor of endoplasmic reticulum stress and potent multitasking transcription factor[14] is one likely target for several reasons. Indeed, endoplasmic reticulum stress is implicated in neurodegenerative diseases and a polymorphism on the *XBP1* promoter is a risk factor for AD.[15] The mRNA of XBP1 is expressed in the brains of adult rodents,[16] although little is known about the detailed pattern of expression and function of XBP1 in the mammalian central nervous system. Furthermore, sparse reports indicate that in hippocampal neurons, XBP1 mRNAs are transported from the nucleus to the dendrites,[17] spliced locally into its active form XBP1s by IRE1 and translated in the manner of local protein synthesis.[18] However, whether XBP1s functionally regulates dendritic spine density and ameliorates synaptic plasticity and memory function in the pathogenic context of AD remain to be determined.

Here we report that therapeutic gene modulation of XBP1s in the hippocampus of AD mice resulted in profound changes of spine density, synaptic plasticity and cognitive function. These changes countervailed Aβ-induced alterations of synaptic plasticity and memory function. We further established that Kalirin-7 (Kal7), a member of the Rho-GEF family that regulates the formation, maturation, and maintenance of dendritic spines,[19] is the main molecular mediator of beneficial effects exerted by XBP1s in AD model.

METHODS SUMMARY

General

Unless indicated otherwise, all data reported in this paper were obtained in blind-coded experiments, in which the investigators who obtained the data were unaware of the specific genotype and treatment of mice, brain slices and cell cultures.

Experimental models

Heterozygous transgenic and nontransgenic mice were from line CRND8[20] and 3xTg-AD.[21] Hippocampal primary neuronal cultures from wild-type rats were treated with medium conditioned by CHO cells that do or do not produce human amyloid-β.[22]

Experimental manipulations

Lentiviral constructs directing expression of no transgene products, XBP1s, EphB2-Flag or green fluorescent protein (GFP) in combination with anti-Kal7 short-hairpin RNAs (shRNAs), anti-EphB2 shRNAs or scrambled control shRNAs were injected stereotaxically into the hippocampus of mice. Neuronal cultures were infected with some of these constructs and stimulated with

Université de Nice-Sophia-Antipolis, Institut de Pharmacologie Moléculaire et Cellulaire, CNRS-UMR7275, Sophia-Antipolis, Valbonne, France. Correspondence: Dr M Cissé, Université de Nice-Sophia-Antipolis, Institut de Pharmacologie Moléculaire et Cellulaire, CNRS-UMR7275, NEUROLOGY, IPMC/CNRS, 660 Route des Lucioles, 06560 Valbonne, France.
E-mail: cisse@ipmc.cnrs.fr
Received 24 March 2016; revised 14 June 2016; accepted 18 July 2016; published online 20 September 2016

Fc-ephrin-B2 or Fc control. Human neuroblastoma cells were transfected with empty vector or a vector encoding Kal7 promoter and treated with Aβ oligomers or vehicle.

Outcome measures

EphB2, GluN1, XBP1s, tubulin, active Rac1, total Rac1 and Kal7 levels in brain tissues or neuronal cultures were determined by western blot. Corresponding transcripts were measured by quantitative polymerase chain reaction with reverse transcription (RT-qPCR). Field recordings from acute hippocampal slices were used to determine synaptic strength (field excitatory postsynaptic potentials (fEPSPs) I/O relationships) and synaptic plasticity long-term potentiation (LTP) at the Schaffer collateral to CA1 pyramidal cell synapses. Learning and memory were assessed in the Morris water maze (MWM) task.

MATERIALS AND METHODS

Preparation of Aβ oligomers

Stably hAPP-transfected CHO cells, which naturally produce Aβ oligomers, were cultured as described.[23] In brief, CHO cells were grown to 80% confluency in 150-mm dishes, washed with PBS and incubated for ~24 h in serum-free Neurobasal A medium. The medium was collected and spun at 1000 rpm for 10 min to eliminate cell debris. Supernatants were concentrated 10-fold with a Centriprep YM-3 (4303; Millipore, Fontenay sous Bois, Île-de-France, France), collected as 1-ml aliquots and stored at − 80 °C.

Primary neuronal culture and treatment

Hippocampi of rat pups (P0) (http://www.criver.com/products-services/basic-research/find-a-model/sprague dawley-rat) were cultured by using the papain dissociation system (LK003150; Worthington) per manufacturer's instructions. Cells were plated in polylysine-coated wells and maintained in serum-free Neurobasal medium (12348-017; Gibco, Thermo Fisher Scientific, Waltham, MA, USA) supplemented with B27 (17504044; Gibco) and antibiotics (15070-063; ThermoFisher Scientific). Half the medium was changed after 5 days in culture. Cells were used after 14 days in culture. More than 95% of the cells were neurons, as determined by staining with an antibody against the neuron-specific marker MAP2 (data not shown). Neuronal cultures were treated with Aβ oligomers from CHO-conditioned medium, control vehicle from untransfected CHO cells, clustered recombinant EphrinB2-Fc (496-EB; R&D Systems, Minneapolis, MN, USA), or control Fc (SA1-600; Thermoscientific). EphrinB2-Fc and control Fc were preclustered with anti-human Fc antibody at 50 ng ml^{-1} in Neurobasal medium at RT for 1 h and applied at final concentrations of 500 ng ml^{-1}. Treatment with anti-Fc antibodies served as an additional control. After treatment, cells were harvested in a lysis buffer (10 mM Tris/HCl, pH 7.5, 150 mM NaCl, 0.5% Triton X-100, 0.5% deoxycholate, 5 mM EDTA) supplemented with a protease inhibitor mixture (Sigma-Aldrich, Saint-Quentin Fallavier, France), spun at 13 000 rpm for 5 min, and frozen at − 80 °C for subsequent determination of protein concentration and western blot analysis.

Immunohistochemistry

Mouse brain sections. After behavioral testing, mice were anesthetized with Pentobarbital (NEMBUTAL, CEVA, Akorn, Lake Forest, IL, USA) and transcardially perfused with 0.9% saline. One hemibrain was drop-fixed in 4% paraformaldehyde for 48 h, and the other hemibrain was immediately frozen at − 70 °C. Sagittal sections (30 μm) were prepared with a sliding microtome and collected for immunohistochemistry. Primary antibodies used were: goat anti-EphB2 (1:500; AF467; R&D Systems), rabbit anti-Kal7 (1:500; Ab-2958 or Ab-2959 (ref. 24)) rabbit anti-XBP1s (1:100; Ab-M186; Santa Cruz Biotechnology, Dallas, TX, USA).

JH2958 or JH2959 antibodies are specific to the last 20 aa C-terminal residues of Kal7, which have been extensively characterized in primary cultured neurons and in hippocampal tissues.[24–28]

Binding of antibodies was detected with biotinylated horse anti-goat (1:2000; BA-9500; Vector Laboratories, Burlingame, CA, USA) or donkey anti-rabbit (1:2000; BA-1000; Vector Laboratories), and incubation with avidin-biotin complex (Vector Laboratories) followed by Streptavidin fluorochrom Alexa594 (1/1000; Molecular Probes, ThermoFisher Scientific). Sections were mounted with Vectashield mounting medium with 4,6-diamidino-2-phenylindole (H1200; Vector Laboratories). Sections labeled with anti-XBP1s were incubated with Alexa594 anti-mouse IgG secondary antibody (1:1000; Molecular Probes, ThermoFisher scientific) and mounted onto slides for analysis with a laser-scanning confocal microscope (LSM 780, Zeiss, Marly-le-Roi cedex, France). The relative numbers of XBP1s neurons were determined by counting positive granule or pyramidal cells in every 5th serial sagittal sections throughout the entire medial-lateral axis of the hippocampus. Confocal images of XBP1s immunoreactivity was analyzed with NIH Image software. All sections were blind coded for analysis.

Human brain sections. Human hippocampal sections embedded in paraffin were immunostained after a dewaxing procedure comprising sequential washing steps with xylene, ethanol and PBS. Sections were immunostained after antigen retrieval in a buffer (Tris, 50 mM; ethylene-diaminetetraacetic acid, 5 mM; pH 8) containing proteinase K (5 μg ml^{-1}) at 37 °C for 30 min. Non-specific binding was blocked by incubation for 2 h in blocking solution (5% BSA in 0.5% TBS-Triton X-100). Sections were incubated overnight at 4 °C with rabbit rabbit anti-Kal7 (1:500 in blocking buffer; Ab-2958 or Ab-2959 (ref. 24)). Biotinylated anti-rabbit secondary antibody (Vector Laboratories) was similarly diluted and applied to the sections for 1 h at room temperature. Sections were revealed as described above.

Imaging of spine density

Imaging was performed on a laser-scanning microscope (LSM 780, Zeiss) by using GFP signal. All dendritic spine counting were done manually with Image J (National Institutes of Health, Bethesda, MD, USA). Sections from lentivirus-injected mice were imaged for dendritic arborization with a ×62 objective and ×3.0 optical zoom. Thickness of z-stack was varied to accommodate the dendritic span of labeled granule or pyramidal cells, with 0.25 μm distance between image planes. Dendritic spines were imaged and analyzed in the outer molecular layers of the dentate gyrus (DG) and in the *stratum radiatum* of CA1 region. Laser intensity and gain were adjusted between sections to accommodate staining efficiency, but the same microscope settings were used within the same section. 4',6-diamidino-2-phenylindole fluorescent immunoreactivity was determined by counting the number of cells stained in four sections each 150 μm apart. The average number of 4',6-diamidino-2-phenylindole-positive cells was defined as 1.0. The infectivity efficiency rate corresponds to the number of GFP-expressing cells reported to 4',6-diamidino-2-phenylindole staining.

Human brain tissue

Frozen tissue. Frozen hippocampal tissue from AD cases and nondemented controls were obtained from the *Lille NeuroBank* collection (Centre de Ressources Biologiques du CHRU de Lille). Nine nondemented individuals (age: 22–80 years; six males, three females; Braak stages 0) and nine AD patients (three males, six females; age: 59–86 years; Braak stages V–VI) were included. Brain pH, postmortem intervals were similar in AD cases and nondemented controls.

Paraffin-embedded tissue. Sections of paraffin-embedded post-mortem brain tissues containing hippocampus from people without cognitive impairments (controls, $n = 5$, 53–92 years) and from patients with AD ($n = 12$, 60–92 years) were obtained from Pitié-Salpêtriere Hospital (Paris, France). Cases met the following criteria: controls, clinical dementia rating (CDR) 0 and Braak stage 0 and AD cases, CDR $\geqslant 4$ and Braak stages V–VI.

Animal models

Mice from line 3xTg-AD are triple transgenic model that are knocked-in for PS1M146V and overexpress Swedish mutated βAPP and P301L tau.[21] We used 3-month-old 3xTg-AD females and control nontransgenic littermates. We used a female-only cohort based on our experience with the 3xTg-AD line and evidence in the literature that females exhibit more extensive amyloid, but similar tau, pathology in this model relative to males.[29] Furthermore, there is an age-dependent sexual dimorphism in cognition and stress response in the 3xTg-AD model, with females performing worse than males shortly after 4 months of age in the MWM task.[30] The transgenic CRND8 is a mouse model of AD-like amyloid pathogenesis that overexpresses an amyloid precursor protein containing the Swedish and Indiana familial AD mutations (K670N/M671L and V717F).[20] We used CRND8 females for biochemical analysis. Naive mice used for knockdown experiments are females from line 129S (Charles River: http://www.criver.

com/products-services/basic-research/find-a-model/129-mice, Saint Germain sur l'Arbresle, Lyon, France). All mouse experiments were approved by the Animal Care and Use Committee of the France Ministry of research under authorization number 00656.02.

Lentivirus production

Lentiviral vectors were based on FUGW.[31] To increase expression of XBP1s or EphB2, a sequence encoding XBP1s or EphB2-Flag was inserted between the NotI sites of the FUGW backbone. PCR was carried out to amplify the mouse XBP1s target sequence inserted within a pcDNA3 vector backbone and driven by a cytomegalo virus promoter as previously described.[32] The pcDNA3-XBP1s vector was a generous gift from Dr Ling Qi laboratory (Michigan Medical School, Ann Arbor, MI, USA). Then, the PCR-amplified sequence encoding XBP1s mouse gene was inserted between the NotI sites of the FUGW vector backbone.[31] Within FUGW vector, the XBP1s sequence is driven by a cytomegalo virus promoter. The same strategy was used to subclone EphB2 into FUGW backbone.

Kal7 or EphB2 expression was reduced with shRNA sequences targeting mouse Kal7 or EphB2 under the U6 promoter. Target sequences were 5′-AGTCTGCAACTCAAGTAGA-3′ for Kal7 and 5′-ACGAGAACATGAACACTAT-3′ for EphB2.[33] The U6-shRNA expression cassette (pSilencer 2.0, Ambion, ThermoFisher Scientific) was inserted between the *Pac*I and *Nhe*I sites of a modified FUGW lentiviral backbone, placing the shRNA cassette upstream of a ubiquitin C promoter directing expression of enhanced GFP. A similar construct expressing a scrambled shRNA was used as a control. Active lentiviral particles were generated by cotransfecting the transfer vector with two helper plasmids, delta8.9 (packaging vector) and VSV-G (envelope vector) into Lenti-X 293 T cell line (632180; Clontech, Mountain View, CA, USA). To prevent contamination by bacteria and mycoplasma, cells were pretreated with Nanomycopulitine reagent (L-X16-010; Biowest, Nuaillé, France). The viral particles were purified from the culture medium by ultracentrifugation. An empty virus was used as control. Viral titers were determined by p24 ELISA (VPK-107; Cell Biolabs, San Diego, CA, USA).

Stereotaxic injection

Two to three-month-old naive, nontransgenic and triple transgenic (3xTg-AD) mice were anesthetized by intraperitoneal injection with a mixture of ketamine (75 mg kg^{-1}) and medetomidine (1 mg kg^{-1}). Mice were placed in a mouse head holder, and lentiviral vectors were stereotactically injected bilaterally into the DG and CA1 region (2–3 µl per site; two sites per hemisphere) with high titers of viral particles (1×10^{10} to 4×10^{10} viral particles) at the following coordinates DG: a/p, −2.1, m/l ±1, d/v, −2.0; CA1: a/p, −2.1, m/l ±1, d/v, −1.5. Viruses expressing XBP1s or EphB2 were mixed at 1:1 ratio with GFP-expressing viruses. We chose this co-infection procedure because large GFP inserts can lead to very low viral titers that are useless for stereotaxic injections and to avoid artifacts on the proper function and trafficking of our proteins of interest that could result from a fusion to GFP. After surgery, anesthetics were reversed with atipamezole (1 mg kg^{-1}). Behavioral assays were carried out 3 months (experiments in naive mice) or 6 months (experiments in transgenic mice) after lentiviral injections.

Protein extraction from tissues

Total tissue lysates from mouse or human brain were obtained by homogenizing isolated hippocampus or microdissected hippocampus (CA1 region and DG) in ice-cold lysis buffer (10 mM Tris/HCl, pH 7.5, 150 mM NaCl, 0.5% Triton X-100, 0.5% deoxycholate, 5 mM EDTA) supplemented with a protease inhibitor mixture (Sigma). Samples were centrifuged at 1000 *g* for 10 min at 4 °C. The supernatant was placed on ice and the pellets were re-homogenized in 0.5 ml of lysis buffer and centrifuged at 1000 *g* for 10 min at 4 °C. The supernatant was combined with the first supernatant collected and centrifuged at 100 000 *g* for 1 h at 4 °C. Supernatant from this last centrifugation was then collected and used to determine the protein concentration of the samples and for western blot analyses.

Immunoblotting

For detection of Kal7, EphB2, total Rac1 and NR1, 50 µg of protein was loaded into each well of a 8% sodium dodecyl sulfate polyacrylamide gel electrophoresis gel. For detection of XBP1s and tubulin, 50 µg of protein was loaded into each well of a 10% sodium dodecyl sulfate polyacrylamide gel electrophoresis gel. Active Rac1 was detected in brain homogenates from lentivirus-injected mice or human tissues with Active Rac1 Pull-Down and Detection Kit (17283; Millipore). For active Rac1 detection, 200–300 µg proteins were pulled-down using 10 µl of PAK1-agarose beads per manufacturer's instructions and loaded into each well of a 16.5% tris tricine gel. Gels were transferred to nitrocellulose membranes and immunoblotted with rabbit anti-Kal7 (1:1000, ab-2958 or ab-2959 (ref. 25)) mouse anti-NR1 (1:1000, Millipore), mouse anti-EphB2 (1:1000, Invitrogen, ThermoFisher Scientific), rabbit anti-XBP1s (1:500; Ab-M186; Santa Cruz Biotechnology), mouse anti-Rac1 (1:1000, Millipore), mouse anti-tubulin (1:1000, SIGMA). Goat anti-rabbit or anti-mouse antibodies (1:5000, Chemicon) were used as secondary antibodies. Protein bands were visualized with SuperSignal West Pico Chemiluminescent Substrate (Thermo Scientific) and quantified densitometrically with Image J software (National Institutes of Health).

ELISA analysis of Aβ levels

Hippocampi were isolated from mice injected with lentiviral particles and homogenized in RIPA buffer (50 mM Tris, pH 7.4, containing 150 mM NaCl, 1 mM EDTA, 1% Triton X-100, 0.5% deoxycholate, 0.1% sodium dodecyl sulfate and protease inhibitor mixture). Samples underwent steps of lysis with a Dounce homogenizer and sonication. After ultracentrifugation (100 000 *g*, 1 h, 4 °C), supernatants were recovered as the soluble fractions. Pellets containing insoluble material were mechanically dissociated in formic acid (70%) and by ultracentrifugation (100 000 *g*, 1 h, 4 °C). Supernatants were stored as the insoluble fraction. Before further analysis, soluble and insoluble fractions were neutralized to pH 7.5 with 1 M Tris-HCl, pH 10.8, containing 25 mM betaine. Sample from insoluble fraction were then homogenized in 5 M guanidine buffer and analyzed by ELISA for levels of human Aβ1-x and Aβ1-42.[34]

qRT-PCR

For quantitative fluorogenic RT-PCR, total RNA was isolated from frozen brain tissues with an RNA shredder and RNeasy Mini kits (74104; Qiagen, Valencia, CA, USA) and stabilized in RNA later buffer (76104; Qiagen). RT reactions containing 120 ng of total RNA were treated with RNase-free DNase (AM2222; Invitrogen, Ambion) for 30 min at 37 °C and each reaction was reverse transcribed with random hexamers and oligo(dT) primers. Diluted reactions were analyzed with SYBR green PCR reagents and a sequence detector (Rotor-gene 6000, Corbett Research, Qiagen). Mouse XBP1s, EphB2, GluN1, or Kal7 mRNA levels were normalized to GAPDH (forward 5′-TGTCCGTCGTGGATCTGAC-3′ and reverse 5′-CCTGCTTCACCACCTTCTTG-3′) or topoisomerase 2 (forward 5′-TGCCTCCATCACACTACAGG-3′ and reverse 5′-CGCTGGTACATTCTCATCAGG-3′). The slope of standard curves, control reactions without RT, and dissociation curves of products indicated adequate PCR quality. The following primers were used to evaluate the levels of various mouse genes: for mEphB2 forward 5′-TTCATGGAGA ACGGATCTCTG-3′ and reverse 5′-GACTGTGAACTGTGAACGCCCATCG-3′; for mKal7 (ref. 35) forward 5′-GATACCATATCCATTGCCTCCAGGACC-3′ and reverse 5′-CCAGGCTGCGCGCGCGCTAAACGTAAG-3′; for mGluN1 forward 5′-TGTCATCCCAAATGACAGGA-3′ and reverse 5′-GGGTTCTTGGTGGATT GTCA-3′; for mXBP1s forward 5′-AGCTTTTACGGGAGAGAAAACTCA-3′ and reverse 5′-GCCTGCACCTGCTGCG-3′.

Generation of Kal7 and EphB2 promoter constructs

To clone rat *EphB2* promoter, 100 ng of rat cortex genomic DNA (http://www.criver.com/products-services/basic-research/find-a-model/sprague dawley-rat) were extracted by using the kit QIAamp DNA mini kit (51304; Qiagen) and added to a high fidelity PCR reaction mix (Promega, Madison, WI, USA) with the forward primer 5′-CTAGCTAGCCTGCCTGGGTG GTTCTCATAGG-3′ containing *Nhe*I restriction site (underlined) and the reverse primer 5′-CCGCTCGAGCATTGATACGCTGCCCGGAG-3′ containing a *Xho*I restriction site (underlined). The 1203 nucleotides long amplicon (corresponding to a rat *EphB2* DNA fragment immediately upstream the translation initiation codon of the reference sequence NM_001127319.1, gene ID: 313633 (https://www.ncbi.nlm.nih.gov/gene/313633) has been cloned between the *Nhe*I and *Xho*I sites of the pGL3 basic vector (containing the sequence coding for luciferase) (E1751; Promega). We used the same strategy to clone rat Kal7 promoter C[35] (100 ng of rat cortex genomic DNA) with the forward primer: 5′-CTAGCTAGCCCTTCCACGTGG AAAGGTGTG-3′ containing a NheI restriction site (underlined) and the reverse primer: 5′-CCGCTCGAGCATCCCACCCTGAACTCATCCTTC-3′ containing *Xho*I restriction site (underlined). We generated a 1213 nucleotides long fragment containing the promoter C of rat Kal7 and corresponding to a

DNA fragment immediately upstream of the translation initiation codon of the reference sequence AF230644.1, gene ID: 84009 (https://www.ncbi.nlm.nih.gov/gene/84009). The DNA fragment was inserted between the *Nhe*I and *Xho*I sites of the pGL3 basic vector. All the constructs were verified by sequencing.

Luciferase assay

Aβ oligomers toxicity assay. SH-SY5Y human neuroblastoma cells (ATCC, CLR-2266) (5–7 day *in vitro*) were transfected using lipofectamine (Invitrogen) with 2.0 μg of the proximal promoter region of rat Kal7 or EphB2 subcloned into the pGL3 basic vector (Promega) according to the manufacturer's instructions or empty pGL3 vector as control. Twenty-four hours later, cells were treated with CHO-derived Aβ oligomers or vehicle for indicated times and analyzed for luciferase activity by using a luciferase assay system (E1500; Promega).

Transcription activity assay. SH-SY5Y human neuroblastoma cells (5–7 day *in vitro*) were cotransfected using lipofectamine (Invitrogen) with 1.0 μg of the proximal promoter region of Kal7 or EphB2 subcloned into the pGL3 reporter vector with FUGW vector encoding XBP1s or empty FUGW control vector. PCR was carried out to amplify the XBP1s target sequence inserted within a pcDNA3 vector backbone and driven by a cytomegalo virus promoter as previously described.[32] The pCDNA3-XBP1s was a generous gift from Dr Ling Qi laboratory (Michigan Medical School). Then, the PCR-amplified sequence encoding XBP1s mouse gene was inserted between the NotI sites of the FUGW vector backbone.[31] Within FUGW vector, the XBP1s sequence is driven by a cytomegalo virus promoter.

Cells were analyzed for luciferase activity 24 h later by using a luciferase assay system (E1500; Promega).

Electrophysiology

Mice injected with lentiviral particles were anesthetized with isoflurane and then decapitated. Brains were quickly removed and placed in ice-cold solution containing (in mM) 2.5 KCl, 1.25 $NaPO_4$, 10 $MgSO_4$, 0.5 $CaCl_2$, 26 $NaHCO_3$, 11 glucose and 234 sucrose (pH, ~7.4; 305 mOsmol). Acute sagittal slices (350 μm thick) were cut with a vibratome (VT 1000S; Leica Microsystems, Bannockburn, IL, USA) and transferred for recovery to a holding chamber containing oxygenated artificial cerebrospinal fluid consisting of 211 mM sucrose, 3.3 mM KCl, 1.3 mM NaH_2PO_4, 0.5 mM $CaCl_2$, 10 mM $MgCl_2$, 26 mM $NaHCO_3$ and 11 mM glucose. Hippocampal slices 124 mM NaCl, 3.3 mM KCl, 1.3 mM NaH_2PO_4, 2.5 mM $CaCl_2$, 1.5 mM $MgCl_2$, 26 mM $NaHCO_3$ and 11 mM glucose (290 mOsmol; gassed with 95% O_2-5% CO_2, pH ~7.4) at 28–30 °C for 30 min before recording. Individual slices were transferred to a submerged recording chamber, where they were maintained at 30 °C and perfused with artificial cerebrospinal fluid at a rate of 1–2 ml min^{-1}. No recordings were made on slices >5 h after dissection. To record fEPSPs, a monopolar electrode was placed in the Schaffer collaterals, and stimulation was applied at 0.066 Hz (every 20 s) with stimulus intensity ranging from 5 to 100 μA, yielding evoked fEPSPs of 0.2–0.5 V. The recording electrode was placed in the stratum radiatum and fEPSPs recorded with a borosilicate micropipette filled with artificial cerebrospinal fluid. Baseline was recorded for a minimum of 30 min or until stable. LTP was induced by stimulation with 100 Hz with three trains of a 1-s tetanus separated by 20 s. Signals were amplified with an Axopatch 200B amplifier (Molecular Devices, Union City, CA, USA) digitized by a Digidata 1322A interface (Axon Instruments, Molecular Devices) and sampled at 10 kHz. Recordings were acquired using Clampex (Molecular Devices) and analyzed with Clampfit (Molecular Devices). The initial fESPS slope in mV ms^{-1} was determined by the software. All experiments were performed by an experimenter blind to treatment or genotype groups. Data on slices from each mouse were averaged, so that measurement on animals and not slices are considered biological replicates.

MWM

For MWM tests and subsequent analyses with AnyMaze software (Stoelting, Wood Dale, IL, USA), experimenters were blinded to the genotype and treatment of mice. Each experiment was replicated one time with two separate cohorts with 1-month interval between tests. The MWM consisted of a pool (90-cm diameter) filled with water (21 ± 1 °C) made opaque with nontoxic white tempera paint powder; the pool was located in a room surrounded by distinct extra-maze cues. Before hidden-platform training, mice were given four pre-training trials in which they had to swim in a rectangular channel and mount a platform hidden 1.5 cm below the surface in the middle of the channel. Mice that did not mount the platform were gently guided to it and were allowed to sit on it for 10 sec before being removed by the experimenter. The maximum time allowed per trial in this task was 90 s. The day after pre-training, mice were trained in the circular water maze. For hidden-platform training, the platform (4 cm radius) was submerged 1.0 cm below the surface. The platform location remained the same throughout hidden-platform training, but the drop location varied semi-randomly between trials. Mice received four trials with 15-min intertrial interval per day for 5 consecutive days. The maximum time allowed per trial in this task was 60 s. If a mouse did not find the platform, it was guided to it and allowed to sit on it for 15 s. A probe trial was performed 72 h after training. The platform was removed and mice were allowed to swim for 60 s. The drop location for probe trials was 180° from where the platform was located during hidden-platform training. After a probe trial, mice were allowed to rest for 1 day before visible platform training was performed. In the latter task, the platform location was marked with a visible cue (10 cm tall black-painted pole) placed on top of the platform. Mice received four training trials in one day. The maximum time allowed per trial in this task was 60 s. For each trial, the platform was moved to a new location, and the drop location varied semi-randomly between trials.

Blind coding and statistical analyses

Investigators who obtained data were blinded to the disease state of human samples and to the genotype and treatment of mice and cell cultures. Sample sizes were chosen on the basis of pilot experiments and our experience with similar experiments. Statistical analyses were performed with GraphPad Prism, R (R Development Core Team), or Statistica (Statsoft, Round Rock, TX, USA). Normal distribution of the data was verified with Shapiro-Wilk's test. Differences between two groups were estimated by two-sided Mann–Whitney test. Differences between more than two groups were assessed by Kruskal–Wallis test. Pairwise comparisons were performed using a Mann–Whitney test with false discovery rate correction or a Nemenyi test. Differences between groups during the learning phase of the MWM test were assessed by repeated measures two-way analysis of variance, followed by Tukey's *post hoc* test. For analysis of variance tests, data were log10-transformed in order to respect homoscedasticity assumptions as assessed by Levene test. When appropriate, univariate Mann–Whitney test was used to test the groups' performances versus chance. Error bars represent s.e.m. Null hypotheses were rejected at the 0.05 level. Statistical significances are represented by the following *P*-values in all figures: $*P < 0.05$; $**P < 0.01$; $***P < 0.001$.

RESULTS

XBP1s ameliorates synaptic plasticity and memory in 3×Tg-AD mice

To determine whether XBP1s ameliorates memory function, we bilaterally injected viral particles expressing XBP1s into the hippocampus of a triple transgenic mouse model of AD (3xTg-AD,[21] referred to as AD hereafter) (Figure 1a). Comparable levels of GFP transduction were observed throughout the hippocampus across all groups (60–75% of neurons were transduced in CA1 region and DG) (Figure 1b and Supplementary Figure 1a–e). Further, XBP1s was highly expressed in neuronal nuclei in CA1 region and DG of AD/XBP1s mice (Figure 1c–e and Supplementary Figure 1f). However, endogenous XBP1s was undetectable in NTG/empty and AD/empty mice, at least by immunohistochemistry, indicating that XBP1s is expressed at very low levels in basal conditions.

Next, we examined whether XBP1s affects spatial learning and memory in the MWM. Remarkably, NTG/empty and AD/XBP1s displayed a normal learning behavior, whereas AD/empty mice showed poor learning performances (Figure 1f). Similarly, in a probe trial, only AD/empty mice did not remember the platform location (Figure 1g) and did not show a persistent memory for the target quadrant (Figure 1h). Overall, AD/XBP1s and NTG/empty mice had comparable learning curves and performed equally well during a probe trial, suggesting that XBP1s ameliorates spatial learning and memory in AD mice. Body weight and swim speeds during the probe trial were comparable among all groups (Supplementary Figure 1g, h). Moreover, all groups performed equally well in the cued MWM (Supplementary Figure 1i),

indicating that learning deficits were not caused by impairments in vision or motor function.

Because neuronal communication and synapses underlie brain activity and as synaptic spines are dynamic structures that regulate neuronal plasticity, we next assessed whether XBP1s ameliorates spatial learning through a positive regulation of spine density. We found that spine density along individual dendrites of CA1 pyramidal neurons was markedly increased in AD/XBP1s and

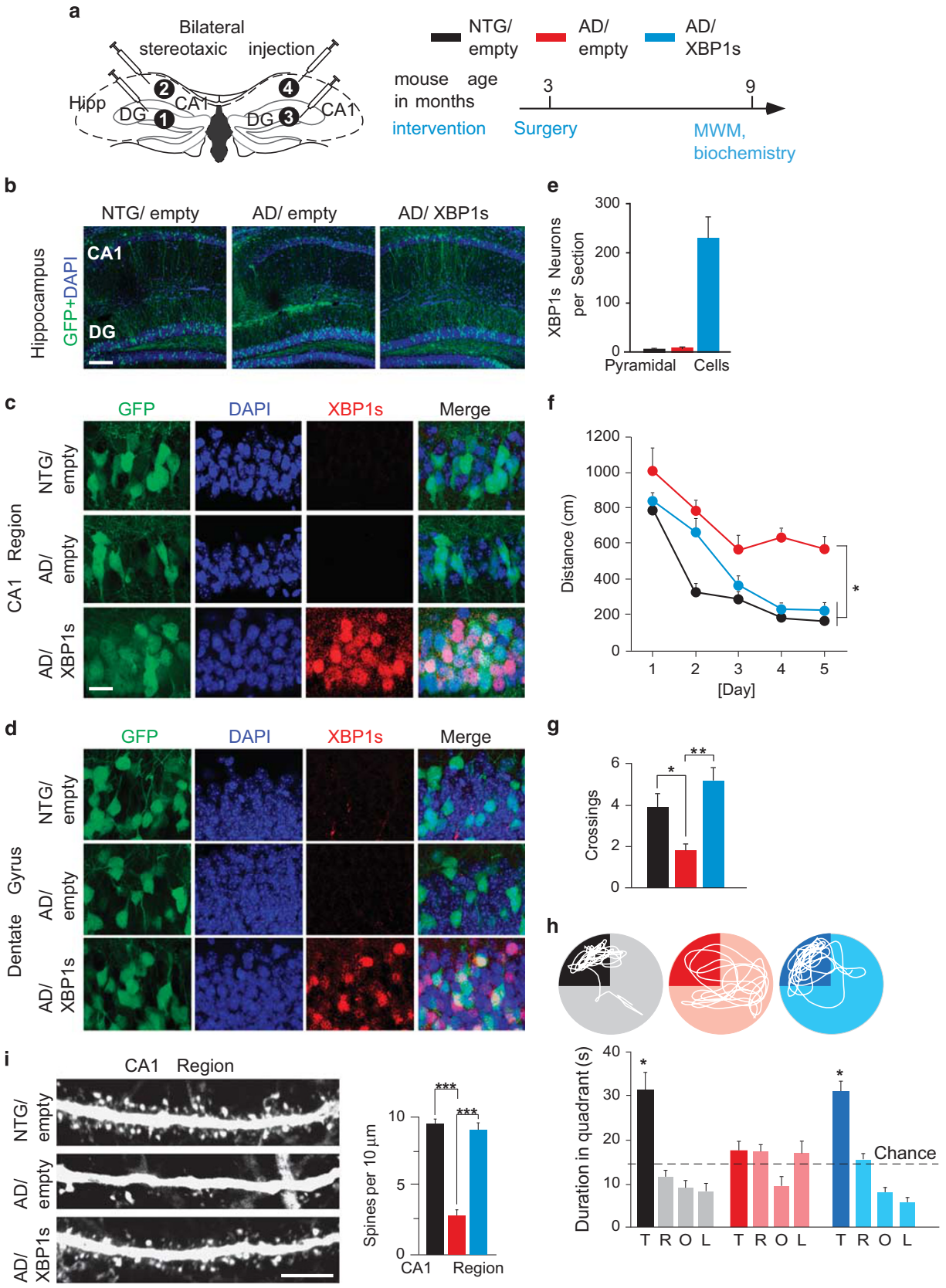

comparable to that of NTG/empty mice. In contrast, AD/empty mice showed a decrease in number of spines (Figure 1i). Thus, expressing XBP1s prevents spine loss in AD mice. Taken together, these data indicate that changes in spine density elicited by XBP1s might underlie the facilitated synaptic plasticity and normal spatial learning behavior of AD mice expressing XBP1s.

Opposite effects of XBP1s and Aβ oligomers on Kal7 signaling

Rho-GEF Kal7 has a major role in the regulation of synapse formation, maturation and maintenance through Rac1 signaling.[24,25,36,37] To gain further insight into the mechanisms by which XBP1s ameliorates neuronal plasticity and memory, we examined XBP1s capacity to modulate Kal7 in neuronal systems. We found that XBP1s significantly increased Kal7 promoter activity in SH-SY5Y cells (Figure 2a), and mRNA and protein levels in primary neurons (Figure 2b, c), suggesting that XBP1s transcriptionally regulates Kal7 *in vitro*.

Evidence suggests that abnormal Kal7 expression may contribute to AD pathogenesis,[38,39] although a direct causal link between Aβ oligomers (Aβos) levels, the alteration of the Kal7 pathway, reduction in spine density and memory deficits has not yet been established. This prompted us to examine hippocampal levels of Kal7 in 3xTg-AD mice. We found that protein and mRNA levels of Kal7 and its activator EphB2[40] were significantly and similarly reduced in AD mice (Figure 2d, e and Supplementary Figure 2). Active Rac1, a downstream molecular mediator of Kal7 signaling, but not total Rac1, was concomitantly reduced (Figure 2f). Similar alterations of the Kal7/Rac1 cascade were observed, starting at 6 months of age, in the hippocampus of CRND8 mice (Supplementary Figure 3a–h), a distinct AD model that displays an overload of Aβ peptides by expressing amyloid precursor protein bearing two familial AD mutations.[20] Together, these results suggest that alterations of the Kal7/Rac1 pathway occur in distinct AD models through mechanisms likely associated to Aβos neurotoxicity.

To test this possibility, we exposed hippocampal primary neuronal cultures to CHO cells-conditioned medium that contains Aβos[22](Supplementary Figure 4) and assessed the effects on Kal7 signaling. One hour treatment with Aβos, but not vehicle, reduced protein expressions (Figure 2g) and transcripts (Figure 2h) of Kal7 and EphB2, but not GluN1, with a subsequent decrease in active Rac1 levels (Figure 2g). Furthermore, Aβos inhibited by 50% activities of EphB2 (Figure 2i) or Kal7 (Figure 2j) promoter. These results identify Aβos as the likely culprit for alterations of the Kal7/Rac1 pathway observed in AD models.

Kal7 pathway is impaired in patients with AD

To examine the relevance of these findings in humans, we compared Kal7 and EphB2 abundance in post-mortem brain samples from patients with Braak and Braak stages V–VI of non-familial AD with samples from healthy control brains. Levels of both proteins were significantly reduced in hippocampal DG and CA1 region in AD cases (Figure 3a–i). In addition, hippocampal samples from AD cases showed a similar decrease in active Rac1 levels (Figure 3j–l). Thus, our data support the notion that alterations of the Kal7/Rac1 pathway underlie synaptic deficits and cognitive decline in AD pathogenesis.

Knockdown of Kal7 levels impairs memory function in naive mice

Next, we sought to determine pathophysiological consequences of reduced Kal7 levels in the hippocampus. To this end, we modulated Kal7 levels in naive mice by generating lentiviral particles carrying shRNAs directed against Kal7 (shKal7)[35] or EphB2 (shEphB2),[33] and a scrambled sequence (shSCR) as control. We separately injected or co-administered these viral particles bilaterally into CA1 region and DG of naive mice (Figure 4a). We observed similar GFP transduction efficiencies in CA1 region and DG across all groups (Supplementary Figure 5a-e). Further comparative analysis showed a selective twofold reduction in Kal7 and/or EphB2 mRNA (Figure 4b) and protein (Supplementary Figure 6) levels in shKal7, shEphB2 and shKal7/shEPhB2 mice relative to shSCR control mice.

Because Kal7 has an essential role in spinogenesis,[41] we measured spine density in CA1 region of the hippocampus. We found a significant decrease of spine numbers in the *stratum radiatum* of shKal7 and shEphB2 mice relative to shSCR control mice (Figure 4c). Notably, the density of dendritic spines was not decreased further in shKal7/shEPhB2 mice, demonstrating that EphB2 and Kal7 act along the same pathway as previously reported.[40] Together, these results reveal that knockdown of Kal7 or EphB2 *per se* is sufficient to reduce spine density. We next assessed synaptic plasticity by measures of LTP at Schaffer collaterals to CA1 pyramidal cells. A robust LTP was induced and sustained in shSCR, but not in shKal7, shEphB2 or shKal7/shEPhB2 mice (Figure 4d). Basal synaptic transmission was not altered by reduction in Kal7, EphB2 or both (Supplementary Figure 5f. Thus, depletion of endogenous Kal7 and/or EphB2 impairs synaptic plasticity through a reduction in spine density.

We evaluated the functional impact of Kal7 or EphB2 knockdown on hippocampus-dependent memory formation in the MWM. shSCR mice traveled shorter distances to reach the platform location (Figure 4e) and showed reduced escape latencies (Supplementary Figure 4a) relative to shKal7, shEphB2 or shKal7/shEPhB2 mice. Likewise, only shSCR mice remembered the platform location (Figure 4f and Supplementary Figure 7b, c) and showed a persistent memory for the target quadrant (Figure 4g) during a probe trial. Visible platform training revealed no altered visual or sensorimotor function (Supplementary Figure 7d). Body weight and swim speed during a probe trial were comparable across all groups (Supplementary Figure 7e, f). Altogether, our data suggest that a reduction of Kal7 expression alters synaptic transmission and thereby impairs hippocampal-dependent spatial memory.

XBP1s ameliorates memory function through Kal7 in 3xTg-AD mice

On the basis of the well-established functional interaction between EphB2 and Kal7,[40,42] we asked whether XBP1s prevents

Figure 1. Expressing XBP1s in the hippocampus rescues cognitive function in 3xTg-AD mice. (**a**) Left, stereotaxic injection of lentiviral vectors into the hippocampus of 3xTg-AD (AD) and nontransgenic (NTG) control mice. Right, timeline of Morris water maze (MWM) test and subsequent biochemical analysis of mice. (**b**) Representative immunofluorescence (IF) images showing GFP-positive cells (green) and DAPI staining (blue). Scale bar, 100 μm. (**c**, **d**) Representative IF images showing XBP1s expression in CA1 region (**c**) and DG (**d**) at high magnification. Scale bar, 20 μm. (**e**) Quantitation of XBP1s expression by IF in the CA1 region. (**f**) Spatial learning curves in the MWM showing distance traveled to reach the hidden platform ($n = 8$ mice per group). Kruskal–Wallis test on day 1: $H = 5.066$, $P > 0.05$; Kruskal–Wallis test on day 5: $H = 10.6082$, $P < 0.001$. Mann–Whitney *post hoc* test: AD/empty versus all other groups on Day 5, $^*P < 0.05$. (**g**) A probe trial showing crossings of the platform location. Kruskal–Wallis test: $H = 10.2162$, $P < 0.001$. Mann–Whitney *post hoc* test. (**h**) A probe trial showing time spent per quadrant in the MWM (T, target; R, right; O, opposite; L, left). Univariate Mann–Whitney test (versus chance): NTG/empty, $U = 21$, $P < 0.05$; AD/empty, $U = 11$, $P > 0.05$; AD/XBP1s, $U = 21$, $P < 0.05$. (**i**) Spine density in CA1 region (Number of slices per mouse/number of mice: 5/7 per group). Kruskal–Wallis test: $H = 40.5554$, $P < 0.001$. Nemenyi *post hoc* test. Scale bar, 10 μm. All values are mean ± s.e.m.

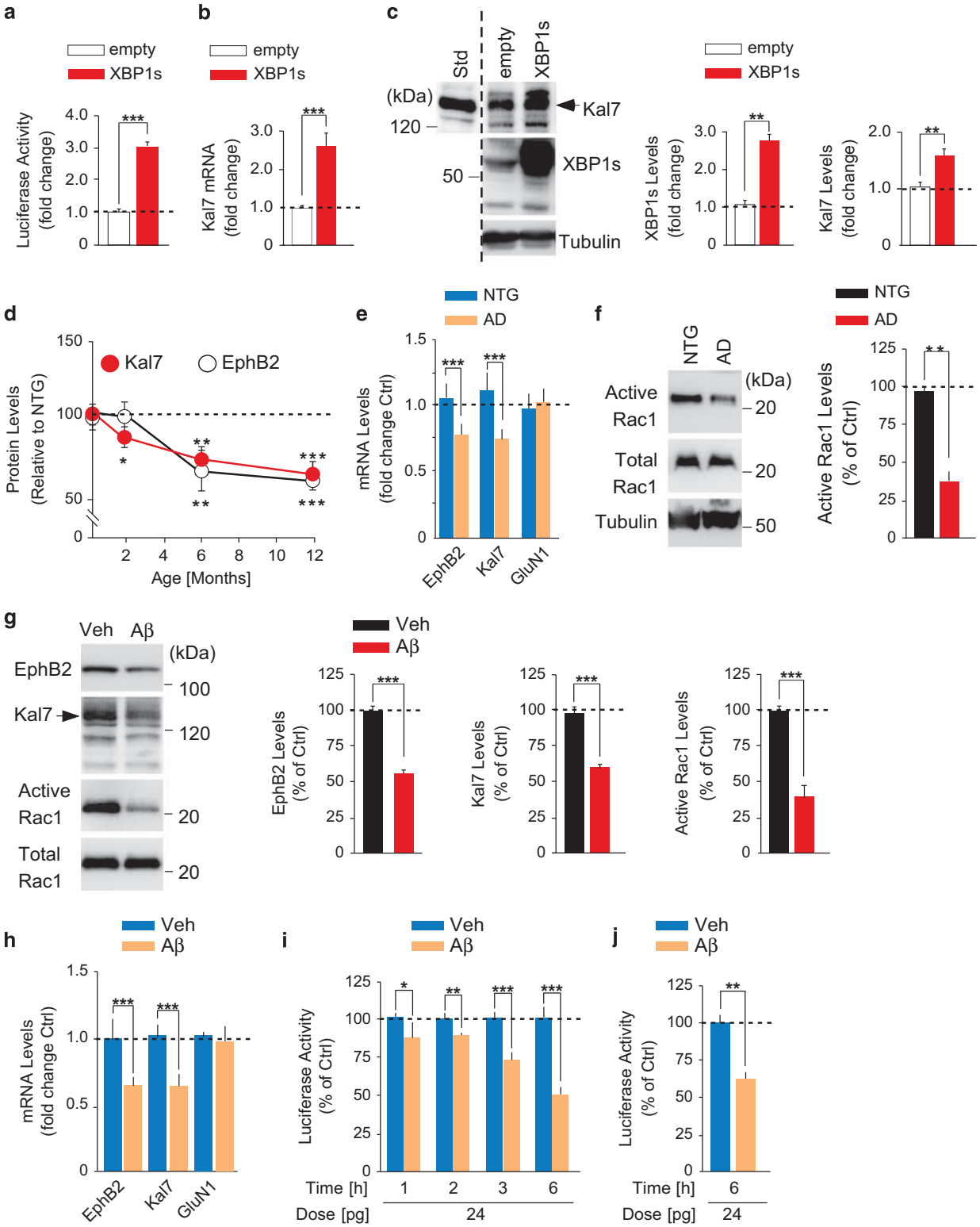

Aβos-induced spine loss and cognitive deficits through EphB2/Kal7 signaling. To answer this question, we first determined if increasing EphB2 levels *per se* in the hippocampus rescues cognitive function in 3xTg-AD mice as it did in the J20-hAPP line.[33] To this end, we generated lentiviral particles which significantly increased EphB2, its tyrosine phosphorylated active form pYEphB2, and active Rac1 levels in primary neurons (Supplementary Figure 8). We injected these viral particles into the hippocampus of 3xTg-AD (AD) and NTG control mice (Supplementary Figure 9a). Protein and mRNA levels of EphB2 were reduced in AD/empty mice and increased in AD/EphB2 mice relative to NTG/empty mice (Supplementary Figure 9b–e). More importantly, expression of EphB2 in AD mice restored Kal7 protein (Supplementary Figure 10a, b) and transcripts (Supplementary

Figure 2. XBP1s and Aβ differently affect Kalirin-7 signaling. (**a**) Luciferase activity of SH-SY5Y human neuroblastoma cells cotransfected with Kalirin-7 (Kal7) promoter and XBP1s or empty vector. Mann–Whitney test: $U = -3.4879$, $P < 0.001$. (**b**, **c**) Kal7 mRNA (**b**) and protein (**c**) levels in hippocampal primary neuronal cultures infected with viral particles expressing XBP1s or no transgene product (empty). Mann–Whitney test: Kal7 mRNA: $U = -3.182$, $P < 0.001$; XBP1s levels: $U = -2.8823$, $P < 0.01$; Kal7 levels: $U = -2.7222$, $P < 0.01$. (**d**) Western blot analysis revealed the timecourse of Kal7 and EphB2 expression in the hippocampus of 3xTg-AD (AD) and nontransgenic (NTG) mice ($n = 9$–11 mice per group). (**e**) qRT-PCR results showing mRNA levels of Kal7, EphB2 and GluN1 in the hippocampus of 6-month-old AD and NTG mice ($n = 9$-11 mice per group). Mann–Whitney test: EphB2: $U = -3.0253$, $P < 0.001$; Kal7: $U = -3.2205$, $P < 0.001$; GluN1: $U = 0.488$, $P > 0.05$. (**f**) Representative western blot images and quantification of total and active Rac1 levels in the hippocampus of 6-month-old AD and NTG mice ($n = 8$–12 mice per group). Mann–Whitney test: $U = -3$, $P < 0.01$. (**g**) Representative western blot images and quantification of EphB2, Kal7, active Rac1 levels in primary neurons exposed to Aβ or vehicle (veh). Mann–Whitney test: EphB2: $U = 2.8924$, $P < 0.001$; Kal7: $U = 2.8824$, $P < 0.001$; active Rac1: $U = -3.0027$, $P < 0.001$. (**h**) qRT-PCR results showing mRNA levels of EphB2, Kal7 and GluN1 in hippocampal primary neuronal cultures exposed to Aβ or vehicle (veh). Mann–Whitney test: EphB2: $U = -2.8868$, $P < 0.001$; Kal7: $U = -3.1044$, $P < 0.001$; GluN1: $U = -0.2312$, $P > 0.05$. (**i**, **j**) Luciferase activity of SH-SY5Y cells transfected with EphB2 (**i**) or Kal7 promoter (**j**), and treated with CHO cells-derived Aβ or vehicle (veh) for indicated times. Mann–Whitney test: EphB2 promoter 1 h, $U = 2.2517$, $P < 0.05$; EphB2 promoter 2 h, $U = 2.9581$, $P < 0.01$; EphB2 promoter 3 h, $U = 3.5762$, $P < 0.001$; EphB2 promoter 6 h, $U = 3.5762$, $P < 0.001$; Kal7 promoter, $U = 2.8823$, $P < 0.01$. For all experiments, $n = 12$ wells per condition from at least five independent experiments. All values are mean ± s.e.m.

Figure 10c) to levels comparable to NTG/empty mice. EphB2-mediated rescue was further evidenced by normal levels of active Rac1 (Supplementary Figure 10d) and dendritic spines in CA1 region (Supplementary Figure 10e, f) and DG (Supplementary Figure 10g, h) in AD/EphB2 mice. There was no difference in spine numbers between NTG/empty and NTG/EphB2 mice, which might indicate a ceiling effect. Consistent with these findings, normalization of spine density by EphB2 resulted in improved synaptic plasticity. Indeed, we found that LTP was impaired in AD/empty mice, but undistinguishable between NTG/empty, NTG/EphB2 and AD/EphB2 mice (Supplementary Figure 11a).

We assessed whether the facilitated synaptic plasticity mediated by EphB2 ameliorates memory function in AD mice. AD/empty mice showed severe deficits in the spatial, hidden-platform component of the MWM, whereas AD/EphB2 mice were protected and performed at NTG/empty control levels (Supplementary Figure 11b). Notably, EphB2 expression did not affect learning in NTG mice. In a probe trial, NTG/empty, NTG/EphB2 and AD/EphB2 mice performed better than AD/empty mice in several outcome measures (Supplementary Figure 11c–e). These results strongly suggest that EphB2 prevents memory deficits in AD mice by restoring Kal7 signaling and further demonstrate that beneficial effects exerted by EphB2 in the J20-hAPP line[33] extend to another transgenic mouse model of AD.

To further characterize XBP1s, we examined protein and mRNA levels in 3xTg-AD, CRND8 and in human brains. At the mRNA level, we observed an increase of XBP1s within 3 months of age in CRND8 and 3xTg-AD mice relative to controls (Supplementary Figure 12a, b). Interestingly, XBP1s mRNAs were reduced to normal levels by 8 months of age. This suggests that a compensatory mechanism might be triggered early during the course of the pathology by Aβos neurotoxicity, but not sustained over time. This hypothesis is supported by experiments showing an increase of XBP1s mRNA in primary neurons acutely treated with exogenous Aβos (Supplementary Figure 12c) and a recent study demonstrating a transient increase with a subsequent decrease of XBP1s in an age-dependent manner in distinct AD models.[43] Meanwhile, we failed to detect endogenous XBP1s protein at either 3- or 8 months of age in CRND8 mice or in AD patients (Supplementary Figure 13). However, XBP1s was previously shown to be altered in AD brains.[43]

As both XBP1s and EphB2 regulate synaptic plasticity and memory function and control Kal7 function in mice, we next assessed whether Kal7 is the main mediator of XBP1s beneficial effects, with EphB2 acting as an intermediate signaling molecule in this cascade. We reasoned that if both EphB2 and Kal7 are downstream effectors of a process initiated by XBP1s to rescue neuronal function, knockdown of endogenous Kal7 or EphB2 would equally reduce or block the neuroprotective effects exerted by XBP1s in AD mice. To test this hypothesis, we designed and tested two different shRNA sequences directed against Kal7 in primary neuronal cultures and chose the most efficient at selectively reducing Kal7 levels for stereotaxic injection (not shown). We co-delivered viral particles expressing no gene product or XBP1s and GFP in combination with shKal7, shEphB2[33] or shSCR into hippocampal CA1 region and DG (Figure 5a) in mice. Number of neurons expressing GFP was comparable in the pyramidal (Figure 5b) and granule cell (Supplementary Figure 14a-c) layers across all groups. Further, XBP1s was efficiently and selectively expressed in these hippocampal regions (Supplementary Figure 14d–e) as assessed by western blot (Supplementary Figure 15) and imunohistochemistry (Supplementary Figure 16), with transcripts of XBP1s and Kal7, but not EphB2 or GluN1, significantly increased in XBP1s-injected mice (Supplementary Figure 17a–d). As expected, EphB2 was significantly reduced in shEphB2-injected mice. However, levels of Kal7 transcripts were comparable between AD/empty/shSCR and AD/XBP1s/shKal7 mice. This likely reflects the opposite effects elicited by XBP1s and shKal7 on Kal7 transcripts.

Further analysis revealed substantially restored dendritic spine numbers in CA1 region (Figure 5c, d) and DG (Supplementary Figure 17e, f) in AD/shSCR/XBP1s mice. Similarly, deficits in LTP were ameliorated in these mice (Figure 5e, f). Strikingly, these rescues were blocked by knockdown of endogenous Kal7, but not EphB2. These data indicate that unlike EphB2, Kal7 is a major downstream mediator of XBP1s-dependent control of synaptic plasticity.

Because AD-related synaptic and cognitive deficits appear to be closely related to Aβos, it is important to determine whether XBP1s, in addition to positively regulate Kal7 function, affects Aβ levels as well. AD mice expressing XBP1s showed a marked decrease in Aβ levels in the hippocampus (Supplementary Figure 18a). At analysis, hAPP mice were 8-9-months old and had not yet formed plaques (not shown), excluding potential effects of XBP1s on plaque formation by sequestering soluble circulating forms of Aβ. This suggests that XBP1s might likely affects Aβ levels by reducing its formation or promoting its clearance. However, XBP1s-injected mice had similar levels of hAPP C-terminal fragments C99 or C83 (Supplementary Figure 18b), hinting that XBP1s could promote a protease activity that degrades Aβ. Several proteases degrade Aβ, including neprilysin,[44–47] insulin-degrading enzyme,[46,47] endothelin-converting enzyme[48] and cathepsin B.[49] We also examined Somatostatin, a neuropeptide that was shown to indirectly modulate Aβ levels through Neprilysin.[50] Alterations in the activities of these proteases or Somatostatin could have profound effects on Aβ accumulation and AD. Therefore we examined these proteases at the mRNA level in the hippocampus of XBP1-injected mice and found no significant differences relative to control mice (Supplementary Figure 18c).

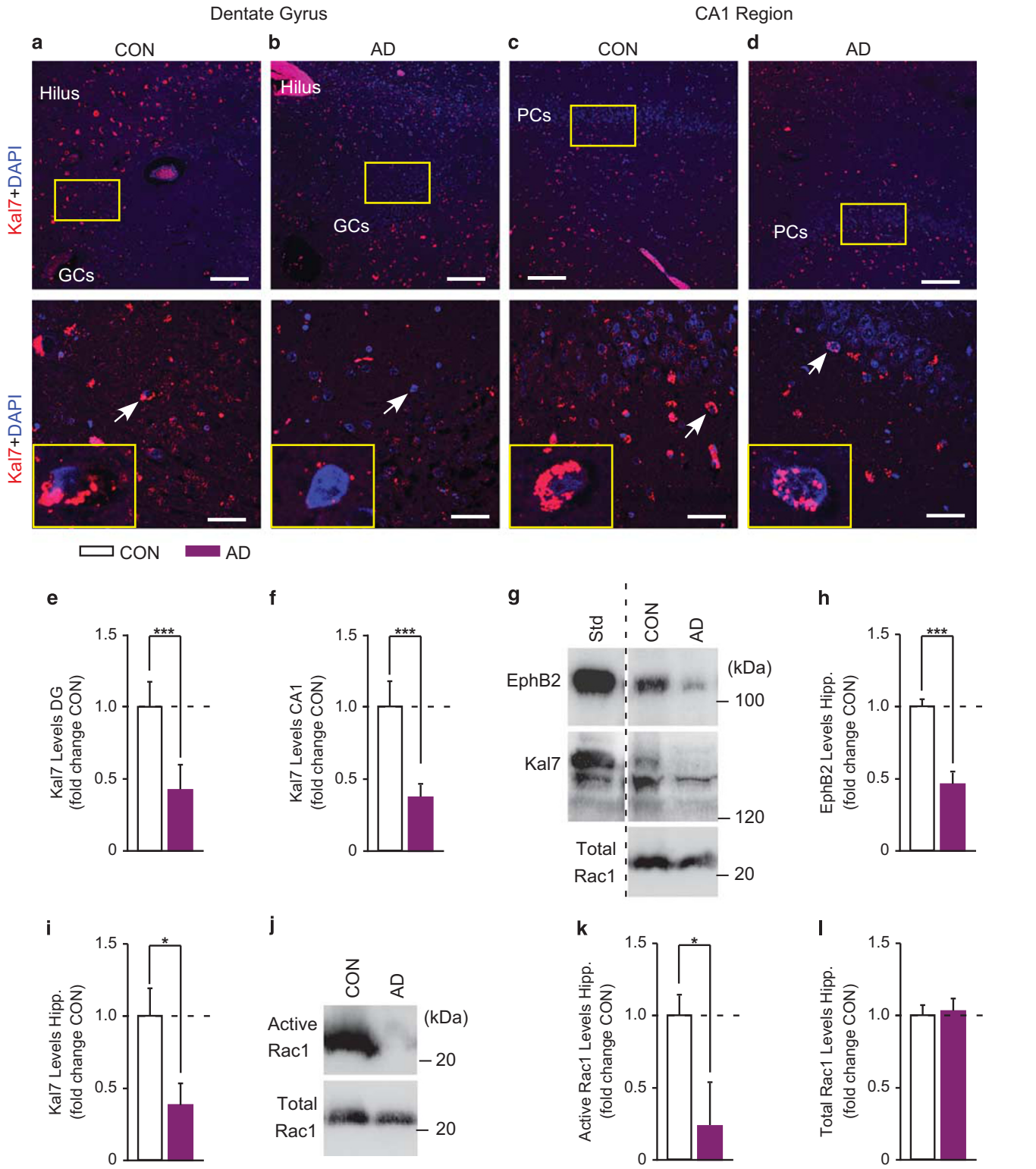

Figure 3. Kalirin-7 levels are reduced in the hippocampus of patients with Alzheimer's disease. (**a**–**d**) Representative immunohistochemical images depicting cytoplasmic Kalirin-7 (Kal7) in neurons of hippocampal dentate gyrus (DG) (**a**, **b**) and CA1 region (**c**, **d**) from patients with Braak and Braak (BB) stages V–VI ($n=12$) compared with healthy BB0 control brains (CON, $n=5$). Scale bar: 100 μm (upper images), 20 μm (lower images). PCs, pyramidal cells; GCs, granule cells. (**e**, **f**) Quantitative assessment of Kal7 levels in **a**–**d**. Mann–Whitney test: Kal7 levels DG: $U=-3.5529$, $P<0.001$; Kal7 levels CA1: $U=-3.5529$, $P<0.001$. (**g**–**l**) Western blot analysis and quantitation of EphB2 (**g**, **h**), Kal7 (**g**, **i**), active and total Rac1 (**j**-**l**) in hippocampal lysates from patients with BBV-VI ($n=9$) compared with healthy BB0 control brains (CON, $n=9$). Mann–Whitney test: EphB2: $U=3.0565$, $P<0.001$; Kal7: $U=-2.313$, $P<0.05$; active Rac1: $U=-2.3834$, $P<0.05$; total Rac1: $U=-0.751$, $P>0.05$. All values are mean ± s.e.m.

Behaviorally, knockdown of Kal7, but not EphB2, prevented XBP1s-mediated rescue of spatial learning behavior in AD mice (Figure 5g and Supplementary Figure 19a). Likewise, AD/empty/shSCR and AD/XBP1s/shKal7 mice had fewer platform area crossings (Figure 5h), and spent less time in the target quadrant during a probe trial (Figure 5i). These mice also spent more time to

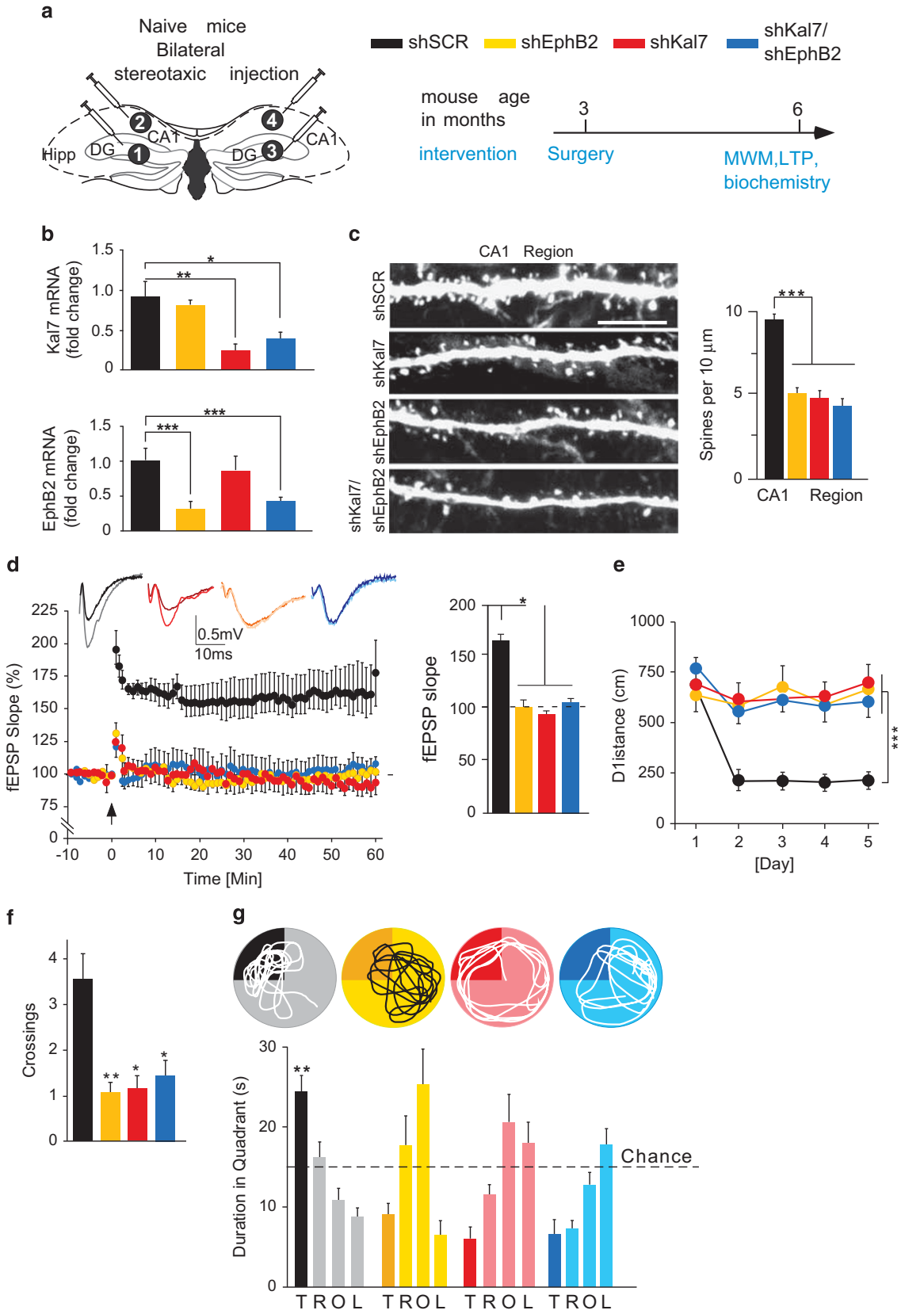

Figure 4. For caption see page on 1572.

reach the platform and gravitated farther from its location (Supplementary Figure 11b, c). Again, shKal7, but not shEphB2, blocked XBP1s-dependent rescue of memory function, indicating that Kal7 is essential to XBP1s-mediated rescue of neuronal plasticity and cognitive function in AD mice. Learning curves during the cued MWM, body weight and swim speeds during a probe trial were similar among all groups (Supplementary Figure 19d-g), excluding experimental biases that could confound the MWM measures.

DISCUSSION

In this study, we have uncovered a key function of XBP1s in the brain, and, we believe, showed for the first time evidence that it alleviates deficits in neuronal plasticity and memory associated with AD pathology. Notably, we have revealed that XBP1s is beneficial through the functional activation of Kal7 that leads to ameliorations of spine density, neuronal plasticity and cognitive function.

An interesting feature is that Kal7 acts as a molecular mediator for both XBP1s and EphB2 to elicit a long-lasting rescue of synaptic plasticity and memory in AD mice. EphB2 is primarily localized at central glutamatergic synapses,[51,52] thus requiring the generation of intracellular fragments or recruitment of an additional molecular partner to mediate a transcriptional activation of Kal7 gene. Meanwhile, XBP1s was mainly detected in the nucleus of principal neurons of CA1 region and DG, consistent with previous reports indicating that XBP1s can function as a transcription factor[53,54] and with our data showing a regulation of Kal7 gene by XBP1s. An intriguing aspect is that endogenous levels of XBP1s were barely detectable in the hippocampus even in the presence of high levels of Aβos. This could be explained by *in vivo* kinetic features underlying a transient expression of the unspliced inactive form of XBP1. This notion is supported by a recent study showing that XBP1 was transiently induced across different ages and AD models.[43] It is also conceivable that expression of XBP1 or its activation by IRE1α occurs under very specific circumstances, stimuli or stress that require certain type of Aβos assemblies but not others. Alternatively, Aβos could repress XBP1 activation and fuel a vicious circle by attenuating the neuronal response to a punctual pathological stress, which over time would overwhelm the neuronal network and compromise its integrity. This is in line with a study showing a disregulation of XBP1 in human AD brains.[43] Notwithstanding Aβos potential effects on XBP1s, it is remarkable that hippocampal delivery of XBP1s was accompanied by a full amelioration of several AD-related functional and anatomical deficits, including alterations in spine density, synaptic plasticity and memory. In a similar vein, the recent work by Martinez *et al*.[55] elegantly showed that expressing XBP1s in wild-type animals enhances neuronal plasticity and hippocampal-dependent memory through a mechanism involving BDNF, as assessed by multiple electrophysiological and behavior outcome measures.

A recent report suggests that XBP1 activates the non-amyloidogenic pathway through the major α-secretase ADAM10 in two distinct animal models.[43] Indeed, an increase in ADAM10 expression/activity could reduce soluble Aβ levels, reduce Aβ plaques and additionally restore learning deficits in AD mice.[56] However, in the current study, AD mice had not yet formed plaques or developed tau pathology[21,57] and did not differ with respect to Aβ levels or APP-derived fragments C83 and C99, excluding the possibility of indirect XBP1s effects, through ADAM10, on plaque load or formations of Aβ and APP carboxy-terminal fragments. Future studies will determine whether XBP1s regulates Aβ levels trough alternates routes such as lysosomal pathway or modulation of β-secretase BACE1 activity/trafficking.

Aβos interacts with and alters the physiological function of several proteins involved in synaptic plasticity and memory, among which α7-nAChR nicotinic receptor,[58] cellular prion protein,[59] EphB2 kinase,[33] human LilrB2[60] or Reelin.[61] The current study revealed that Kal7 depletion in animal models and human AD brains is induced, at least partly, by Aβos neurotoxicity. Nonetheless, it is unclear whether this effect exclusively depends on a direct interaction between Aβos and Kal7 or implicates EphB2 depletion induced by Aβos, which subsequently reduces Kal7 transcripts. These possibilities are not mutually exclusive.

Although we cannot rule out the possibility that other Kalirin family members might have a role in synaptic function and memory, evidence from this study suggest that Kal7 constitutes the main molecular mediator of XBP1s-dependent amelioration of cognitive function: a partial reduction of endogenous Kal7 mimicked Aβos-induced hippocampal neuronal dysfunction and memory deficits; expressing XBP1s in the hippocampus restored Kal7 function and ameliorated several Aβos-associated neuronal alterations in mice; and a knockdown of Kal7 completely blocked XBP1s beneficial effects on synaptic plasticity and memory. This is consistent with previous reports showing that Kal7 promotes spine formation and maturation in different model systems and is critical for hippocampal-based learning and memory.[24,25,37] Interestingly, we showed that Kal7 is reduced in the hippocampus of human AD cases, which has been hinted at by previous studies showing a reduction at the mRNA level,[38,39] indicating that alterations in Kal7 function might genuinely contribute to the human pathology. Local delivery of XBP1s was proved efficient as a potential therapeutic mean in several neurodegenerative diseases. Indeed, XBP1s alleviated pathologies in Parkinson's and Huntington's models,[62,63] demonstrating that artificial engagement of XBP1s-dependent responses may have therapeutic potential to treat a variety of pathological conditions.

Aβos from different sources[64,65] have been shown to affect spine density through a myriad of signaling pathways that ultimately activate cofilin through LIMK, Rac1 and calcineurin,[64] the G(q) protein-coupled P2Y(2) nucleotide receptor,[66] murine PirB (paired immunoglobulin-like receptor B) and its human ortholog LilrB2.[60] Therefore, we expect that treatment with Aβos would likely activate most if not all of these different pathways. It would be interesting in future studies to determine whether XBP1s

Figure 4. Reducing Kalirin-7 levels induces synaptic and cognitive deficits in naive mice. (**a**) Left, bilateral stereotaxic injection of lentiviral vectors into the hippocampus of naive mice. Right, timeline of Morris water maze (MWM) test and subsequent biochemical analysis of mice. (**b**) qRT-PCR analysis of EphB2 and Kal7 transcripts in the whole hippocampus ($n = 5$–6 mice per group). Kruskal–Wallis test: EphB2: $H = 14.4855$, $P < 0.001$; Kal7: $H = 14.3666$, $P < 0.001$. Mann–Whitney *post hoc* test. (**c**) Spine density in CA1 region (Number of slice per mouse/number of mice: 5/7 per group). Kruskal–Wallis test: $H = 50.0822$, $P < 0.001$. Nemenyi *post hoc* test. Scale bar, 10 μm. (**d**) Field excitatory postsynaptic potential (fEPSP) slopes in CA1 region ($n = 3$–4 slices per mouse from 6–7 mice per group). Kruskal–Wallis test: $H = 9.5095$, $P < 0.05$. Mann–Whitney *post hoc* test on the last 10 min of data. (**e**) Spatial learning curves in the MWM showing distance traveled to reach the hidden platform ($n = 12$ mice per group). Repeated measures two-way ANOVA: $F_{12,176} = 4.09$, $P < 0.001$. Tukey HSD post hoc test: shSCR versus all other groups on Day 5, $^{***}P < 0.001$. (**f**) A probe trial showing number of platform location crossings. Kruskal–Wallis test: $H = 12.7346$, $P < 0.001$. Mann–Whitney *post hoc* test: NTG/shSCR versus all other groups, $^{*}P < 0.05$; $^{**}P < 0.01$. (**g**) A probe trial showing the time spent per quadrant (T, target quadrant; R, right; O, opposite; L, left of target). Univariate Mann–Whitney test (versus chance): $U = 65$, $P < 0.01$. All values are mean ± s.e.m.

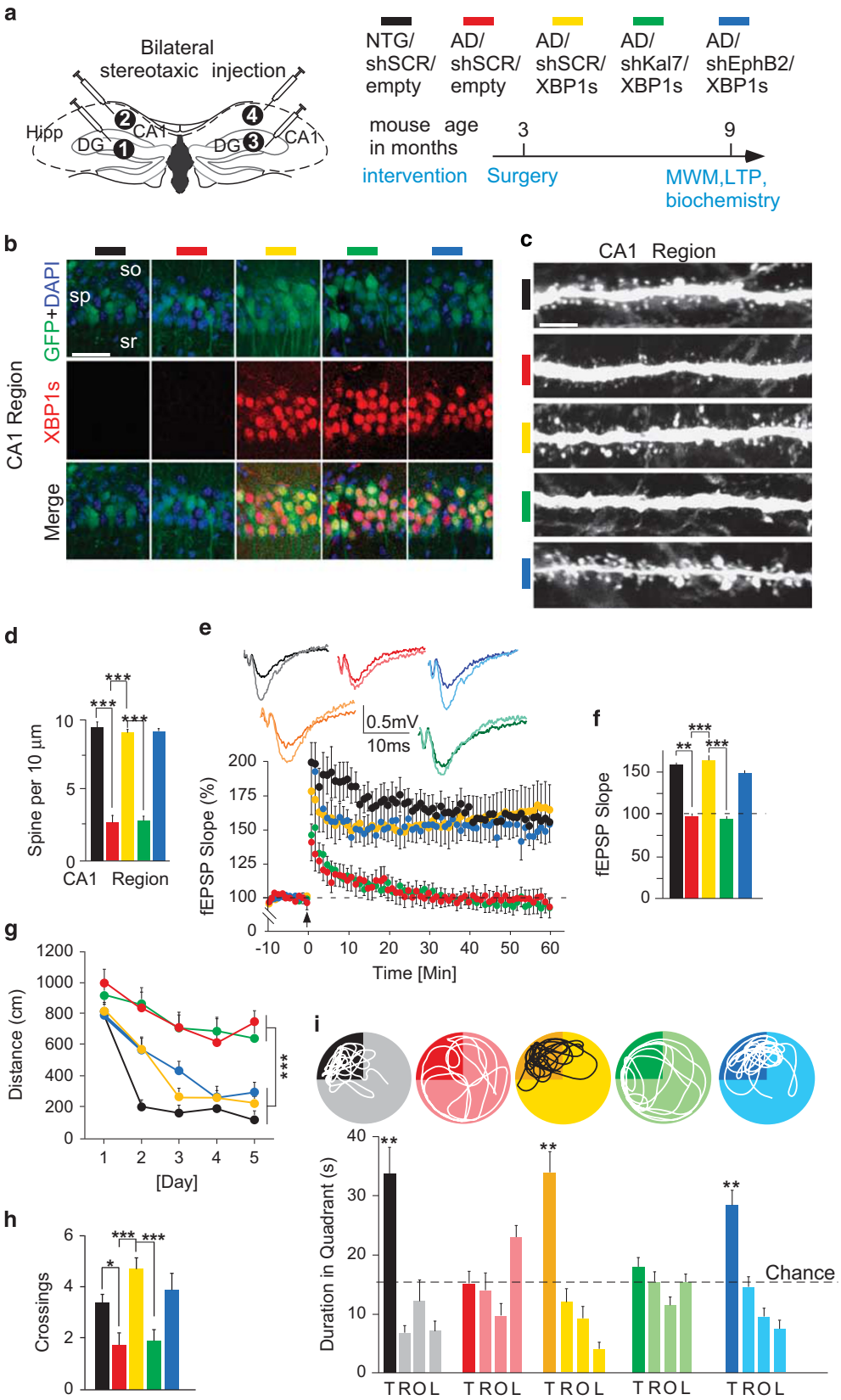

Figure 5. For caption see page on 1574.

beneficial effects are specifically controlled by a cofilin-mediated regulation.

In conclusion, we propose a model (Supplementary Figure 19h) in which XBP1s protects against Aβos-induced pathology and pinpoint Kal7 as a key molecular mediator of these beneficial effects. This uncovers a potential new strategy for therapeutic intervention of human conditions associated with memory impairment.

Figure 5. Depletion of Kalirin-7, but not EphB2, abolishes XBP1s-associated rescue of synaptic plasticity and memory in 3xTg-AD mice. (**a**) Left, stereotaxic injection of lentiviral vectors into the hippocampus of 3xTg-AD (AD) and nontransgenic (NTG) control mice. Right, timeline of Morris water maze (MWM) test and subsequent biochemical analysis of mice. (**b**) Immunofluorescence images depicting GFP-positive cells with DAPI and XBP1s stainings in CA1 region. Scale bar, 20 μm. (**c**, **d**) Spine density in CA1 region (number of slice per mouse/number of mice: 5/7 per group). Kruskal–Wallis test: $H = 74.2712$, $P < 0.001$. Nemenyi *post hoc* test. Scale bar, 10 μm. (**e**, **f**) Field excitatory postsynaptic potential (fEPSP) slopes and average slopes of fEPSP during the last 10 min in CA1 region ($n = 2$–3 slices per mouse from 6–7 mice per group). Kruskal–Wallis test: $H = 25.6637$, $P < 0.001$. Mann–Whitney *post hoc* test on the last 10 min of data. (**g**) Spatial learning curves in the MWM showing distances traveled to reach the hidden-platform location ($n = 12$ mice per group). Repeated measures two-way ANOVA: $F_{16,220} = 4.385$, $P < 0.001$. Tukey HSD *post hoc* test on day 5: NTG/shSCR/empty, AD/shSCR/XBP1s, AD/shEphB2/XBP1s versus AD/shSCR/empty, AD/shKal7/XBP1s, $^{***}P < 0.001$. (**h**) A Probe trial showing platform location crossings. Kruskal–Wallis test: $H = 21.114$, $P < 0.001$. Mann–Whitney *post hoc* test. (**i**) A Probe trial showing the time spent per quadrant (T, target quadrant; R, right; O, opposite; L, left of target). Univariate Mann–Whitney test (versus chance); NTG/shSCR: $U = 75$, $P < 0.01$; AD/XBP1s: $U = 78$, $P < 0.01$; AD/XBP1s/shEphB2: $U = 78$, $P < 0.01$. All values are mean ± s.e.m.

CONFLICT OF INTEREST

The authors declare no conflict of interest.

ACKNOWLEDGMENTS

We thank BA Eipper for providing antibodies and vectors encoding Kal7, P Frazer and P St George-Hyslop for providing CRND8 mice, F Brau for assistance with confocal microscopy, N Robakis for providing vector encoding EphB2 receptor, Paris GIE Neuro-CEB and Lille NeuroBank for human tissues, Ephy-Science for electrophysiology recordings, L Qi for providing vector encoding XBP1s, F Aguila for preparation of graphics. This work was supported by the LABEX (Laboratory of Excellence, investment for the future program) DISTALZ (Development of Innovative Strategies for a Transdisciplinary approach to AD), by FHU OncoAge, by 'Conseil Départemental des Alpes Maritimes', and by a grant from France Alzheimer's Association.

AUTHOR CONTRIBUTIONS

MC designed the research. MC, ED, JD, CD, XM, YG and IL performed experiments. TL helped design behavioral tests and conducted statistical analysis. All authors provided comments on the manuscript. MC and FC wrote and edited the paper. MC and FC supervised the project.

REFERENCES

1 Busquets-Garcia A, Gomis-Gonzalez M, Guegan T, Agustin-Pavon C, Pastor A, Mato S *et al.* Targeting the endocannabinoid system in the treatment of fragile X syndrome. *Nat Med* 2013; **19**: 603–607.
2 Mukai J, Dhilla A, Drew LJ, Stark KL, Cao L, MacDermott AB *et al.* Palmitoylation-dependent neurodevelopmental deficits in a mouse model of 22q11 microdeletion. *Nat Neurosci* 2008; **11**: 1302–1310.
3 Hayashi-Takagi A, Takaki M, Graziane N, Seshadri S, Murdoch H, Dunlop AJ *et al.* Disrupted-in-Schizophrenia 1 (DISC1) regulates spines of the glutamate synapse via Rac1. *Nat Neurosci* 2010; **13**: 327–332.
4 Jimenez-Mateos EM, Engel T, Merino-Serrais P, McKiernan RC, Tanaka K, Mouri G *et al.* Silencing microRNA-134 produces neuroprotective and prolonged seizure-suppressive effects. *Nat Med* 2012; **18**: 1087–1094.
5 Wei W, Nguyen LN, Kessels HW, Hagiwara H, Sisodia S, Malinow R. Amyloid beta from axons and dendrites reduces local spine number and plasticity. *Nat Neurosci* 2010; **13**: 190–196.
6 Zhou YD, Lee S, Jin Z, Wright M, Smith SE, Anderson MP. Arrested maturation of excitatory synapses in autosomal dominant lateral temporal lobe epilepsy. *Nat Med* 2009; **15**: 1208–1214.
7 Blennow K, de Leon MJ, Zetterberg H. Alzheimer's disease. *Lancet* 2006; **368**: 387–403.
8 Scheff SW, Price DA, Schmitt FA, DeKosky ST, Mufson EJ. Synaptic alterations in CA1 in mild Alzheimer disease and mild cognitive impairment. *Neurology* 2007; **68**: 1501–1508.
9 Um JW, Kaufman AC, Kostylev M, Heiss JK, Stagi M, Takahashi H *et al.* Metabotropic glutamate receptor 5 is a coreceptor for Alzheimer abeta oligomer bound to cellular prion protein. *Neuron* 2013; **79**: 887–902.
10 Mairet-Coello G, Courchet J, Pieraut S, Courchet V, Maximov A, Polleux F. The CAMKK2-AMPK kinase pathway mediates the synaptotoxic effects of Abeta oligomers through Tau phosphorylation. *Neuron* 2013; **78**: 94–108.
11 Li S, Jin M, Zhang D, Yang T, Koeglsperger T, Fu H *et al.* Environmental novelty activates beta2-adrenergic signaling to prevent the impairment of hippocampal LTP by Abeta oligomers. *Neuron* 2013; **77**: 929–941.
12 Segal M. Dendritic spines and long-term plasticity. *Nat Rev Neurosci* 2005; **6**: 277–284.
13 Chen Y, Rex CS, Rice CJ, Dube CM, Gall CM, Lynch G *et al.* Correlated memory defects and hippocampal dendritic spine loss after acute stress involve corticotropin-releasing hormone signaling. *Proc Natl Acad Sci USA* 2010; **107**: 13123–13128.
14 Yoshida H, Matsui T, Yamamoto A, Okada T, Mori K. XBP1 mRNA is induced by ATF6 and spliced by IRE1 in response to ER stress to produce a highly active transcription factor. *Cell* 2001; **107**: 881–891.
15 Hetz C, Mollereau B. Disturbance of endoplasmic reticulum proteostasis in neurodegenerative diseases. *Nat Rev Neurosci* 2014; **15**: 233–249.
16 Paschen W, Yatsiv I, Shoham S, Shohami E. Brain trauma induces X-box protein 1 processing indicative of activation of the endoplasmic reticulum unfolded protein response. *J Neurochem* 2004; **88**: 983–992.
17 Hayashi A, Kasahara T, Iwamoto K, Ishiwata M, Kametani M, Kakiuchi C *et al.* The role of brain-derived neurotrophic factor (BDNF)-induced XBP1 splicing during brain development. *J Biol Chem* 2007; **282**: 34525–34534.
18 Sutton MA, Schuman EM. Local translational control in dendrites and its role in long-term synaptic plasticity. *J Neurobiol* 2005; **64**: 116–131.
19 Mandela P, Ma XM. Kalirin, a key player in synapse formation, is implicated in human diseases. *Neural Plast* 2012; **2012**: 728161.
20 Chishti MA, Yang DS, Janus C, Phinney AL, Horne P, Pearson J *et al.* Early-onset amyloid deposition and cognitive deficits in transgenic mice expressing a double mutant form of amyloid precursor protein 695. *J Biol Chem* 2001; **276**: 21562–21570.
21 Oddo S, Caccamo A, Shepherd JD, Murphy MP, Golde TE, Kayed R *et al.* Triple-transgenic model of Alzheimer's disease with plaques and tangles: intracellular Abeta and synaptic dysfunction. *Neuron* 2003; **39**: 409–421.
22 Guillot-Sestier MV, Sunyach C, Druon C, Scarzello S, Checler F. The alpha-secretase-derived N-terminal product of cellular prion, N1, displays neuroprotective function in vitro and in vivo. *J Biol Chem* 2009; **284**: 35973–35986.
23 Walsh DM, Klyubin I, Fadeeva JV, Cullen WK, Anwyl R, Wolfe MS *et al.* Naturally secreted oligomers of amyloid beta protein potently inhibit hippocampal long-term potentiation in vivo. *Nature* 2002; **416**: 535–539.
24 Ma XM, Kiraly DD, Gaier ED, Wang Y, Kim EJ, Levine ES *et al.* Kalirin-7 is required for synaptic structure and function. *J Neurosci* 2008; **28**: 12368–12382.
25 Ma XM, Wang Y, Ferraro F, Mains RE, Eipper BA. Kalirin-7 is an essential component of both shaft and spine excitatory synapses in hippocampal interneurons. *J Neurosci* 2008; **28**: 711–724.
26 Penzes P, Johnson RC, Alam MR, Kambampati V, Mains RE, Eipper BA. An isoform of kalirin, a brain-specific GDP/GTP exchange factor, is enriched in the post-synaptic density fraction. *J Biol Chem* 2000; **275**: 6395–6403.
27 Xin X, Wang Y, Ma XM, Rompolas P, Keutmann HT, Mains RE *et al.* Regulation of Kalirin by Cdk5. *J Cell Sci* 2008; **121**: 2601–2611.
28 Kiraly DD, Lemtiri-Chlieh F, Levine ES, Mains RE, Eipper BA. Kalirin binds the NR2B subunit of the NMDA receptor, altering its synaptic localization and function. *J Neurosci* 2011; **31**: 12554–12565.
29 Hirata-Fukae C, Li HF, Hoe HS, Gray AJ, Minami SS, Hamada K *et al.* Females exhibit more extensive amyloid, but not tau, pathology in an Alzheimer transgenic model. *Brain Res* 2008; **1216**: 92–103.
30 Clinton LK, Billings LM, Green KN, Caccamo A, Ngo J, Oddo S *et al.* Age-dependent sexual dimorphism in cognition and stress response in the 3xTg-AD mice. *Neurobiol Dis* 2007; **28**: 76–82.
31 Lois C, Hong EJ, Pease S, Brown EJ, Baltimore D. Germline transmission and tissue-specific expression of transgenes delivered by lentiviral vectors. *Science* 2002; **295**: 868–872.
32 Duplan E, Giaime E, Viotti J, Sevalle J, Corti O, Brice A *et al.* ER-stress-associated functional link between Parkin and DJ-1 via a transcriptional cascade involving the tumor suppressor p53 and the spliced X-box binding protein XBP-1. *J Cell Sci* 2013; **126**: 2124–2133.

33 Cisse M, Halabisky B, Harris J, Devidze N, Dubal DB, Sun B *et al.* Reversing EphB2 depletion rescues cognitive functions in Alzheimer model. *Nature* 2011; **469**: 47–52.
34 Lauritzen I, Pardossi-Piquard R, Bauer C, Brigham E, Abraham JD, Ranaldi S *et al.* The beta-secretase-derived C-terminal fragment of betaAPP, C99, but not Abeta, is a key contributor to early intraneuronal lesions in triple-transgenic mouse hippocampus. *J Neurosci* 2012; **32**: 16243–16255a.
35 Mains RE, Kiraly DD, Eipper-Mains JE, Ma XM, Eipper BA. Kalrn promoter usage and isoform expression respond to chronic cocaine exposure. *BMC Neurosci* 2011; **12**: 20.
36 Penzes P, Johnson RC, Sattler R, Zhang X, Huganir RL, Kambampati V *et al.* The neuronal Rho-GEF Kalirin-7 interacts with PDZ domain-containing proteins and regulates dendritic morphogenesis. *Neuron* 2001; **29**: 229–242.
37 Xie Z, Srivastava DP, Photowala H, Kai L, Cahill ME, Woolfrey KM *et al.* Kalirin-7 controls activity-dependent structural and functional plasticity of dendritic spines. *Neuron* 2007; **56**: 640–656.
38 Youn H, Jeoung M, Koo Y, Ji H, Markesbery WR, Ji I *et al.* Kalirin is under-expressed in Alzheimer's disease hippocampus. *J Alzheimers Dis* 2007; **11**: 385–397.
39 Murray PS, Kirkwood CM, Gray MC, Ikonomovic MD, Paljug WR, Abrahamson EE *et al.* beta-Amyloid 42/40 ratio and kalirin expression in Alzheimer disease with psychosis. *Neurobiol Aging* 2012; **33**: 2807–2816.
40 Penzes P, Beeser A, Chernoff J, Schiller MR, Eipper BA, Mains RE *et al.* Rapid induction of dendritic spine morphogenesis by trans-synaptic ephrinB-EphB receptor activation of the Rho-GEF kalirin. *Neuron* 2003; **37**: 263–274.
41 Ma XM, Huang J, Wang Y, Eipper BA, Mains RE. Kalirin, a multifunctional Rho guanine nucleotide exchange factor, is necessary for maintenance of hippocampal pyramidal neuron dendrites and dendritic spines. *J Neurosci* 2003; **23**: 10593–10603.
42 Murata Y, Constantine-Paton M. Postsynaptic density scaffold SAP102 regulates cortical synapse development through EphB and PAK signaling pathway. *J Neurosci* 2013; **33**: 5040–5052.
43 Reinhardt S, Schuck F, Grosgen S, Riemenschneider M, Hartmann T, Postina R *et al.* Unfolded protein response signaling by transcription factor XBP-1 regulates ADAM10 and is affected in Alzheimer's disease. *FASEB J* 2014; **28**: 978–997.
44 Iwata N, Tsubuki S, Takaki Y, Shirotani K, Lu B, Gerard NP *et al.* Metabolic regulation of brain Abeta by neprilysin. *Science* 2001; **292**: 1550–1552.
45 Shirotani K, Tsubuki S, Iwata N, Takaki Y, Harigaya W, Maruyama K *et al.* Neprilysin degrades both amyloid beta peptides 1-40 and 1-42 most rapidly and efficiently among thiorphan- and phosphoramidon-sensitive endopeptidases. *J Biol Chem* 2001; **276**: 21895–21901.
46 Leissring MA, Farris W, Chang AY, Walsh DM, Wu X, Sun X *et al.* Enhanced proteolysis of beta-amyloid in APP transgenic mice prevents plaque formation, secondary pathology, and premature death. *Neuron* 2003; **40**: 1087–1093.
47 Caccamo A, Oddo S, Sugarman MC, Akbari Y, LaFerla FM. Age- and region-dependent alterations in Abeta-degrading enzymes: implications for Abeta-induced disorders. *Neurobiol Aging* 2005; **26**: 645–654.
48 Choi DS, Wang D, Yu GQ, Zhu G, Kharazia VN, Paredes JP *et al.* PKCepsilon increases endothelin converting enzyme activity and reduces amyloid plaque pathology in transgenic mice. *Proc Natl Acad Sci USA* 2006; **103**: 8215–8220.
49 Mueller-Steiner S, Zhou Y, Arai H, Roberson ED, Sun B, Chen J *et al.* Antiamyloidogenic and neuroprotective functions of cathepsin B: implications for Alzheimer's disease. *Neuron* 2006; **51**: 703–714.
50 Saito T, Iwata N, Tsubuki S, Takaki Y, Takano J, Huang SM *et al.* Somatostatin regulates brain amyloid beta peptide Abeta42 through modulation of proteolytic degradation. *Nat Med* 2005; **11**: 434–439.
51 Nolt MJ, Lin Y, Hruska M, Murphy J, Sheffler-Colins SI, Kayser MS *et al.* EphB controls NMDA receptor function and synaptic targeting in a subunit-specific manner. *J Neurosci* 2011; **31**: 5353–5364.
52 Kayser MS, McClelland AC, Hughes EG, Dalva MB. Intracellular and trans-synaptic regulation of glutamatergic synaptogenesis by EphB receptors. *J Neurosci* 2006; **26**: 12152–12164.
53 He Y, Sun S, Sha H, Liu Z, Yang L, Xue Z *et al.* Emerging roles for XBP1, a sUPeR transcription factor. *Gene Expr* 2010; **15**: 13–25.
54 Hetz C, Martinon F, Rodriguez D, Glimcher LH. The unfolded protein response: integrating stress signals through the stress sensor IRE1alpha. *Physiol Rev* 2011; **91**: 1219–1243.
55 Martinez G, Vidal RL, Mardones P, Serrano FG, Ardiles AO, Wirth C *et al.* Regulation of Memory Formation by the Transcription Factor XBP1. *Cell Rep* 2016; **14**: 1382–1394.
56 Postina R, Schroeder A, Dewachter I, Bohl J, Schmitt U, Kojro E *et al.* A disintegrin-metalloproteinase prevents amyloid plaque formation and hippocampal defects in an Alzheimer disease mouse model. *J Clin Invest* 2004; **113**: 1456–1464.
57 Oddo S, Caccamo A, Kitazawa M, Tseng BP, LaFerla FM. Amyloid deposition precedes tangle formation in a triple transgenic model of Alzheimer's disease. *Neurobiol Aging* 2003; **24**: 1063–1070.
58 Dineley KT, Bell KA, Bui D, Sweatt JD. beta -Amyloid peptide activates alpha 7 nicotinic acetylcholine receptors expressed in Xenopus oocytes. *J Biol Chem* 2002; **277**: 25056–25061.
59 Lauren J, Gimbel DA, Nygaard HB, Gilbert JW, Strittmatter SM. Cellular prion protein mediates impairment of synaptic plasticity by amyloid-beta oligomers. *Nature* 2009; **457**: 1128–1132.
60 Kim T, Vidal GS, Djurisic M, William CM, Birnbaum ME, Garcia KC *et al.* Human LilrB2 is a beta-amyloid receptor and its murine homolog PirB regulates synaptic plasticity in an Alzheimer's model. *Science* 2013; **341**: 1399–1404.
61 Pujadas L, Rossi D, Andres R, Teixeira CM, Serra-Vidal B, Parcerisas A *et al.* Reelin delays amyloid-beta fibril formation and rescues cognitive deficits in a model of Alzheimer's disease. *Nat Commun* 2014; **5**: 3443.
62 Valdes P, Mercado G, Vidal RL, Molina C, Parsons G, Court FA *et al.* Control of dopaminergic neuron survival by the unfolded protein response transcription factor XBP1. *Proc Natl Acad Sci USA* 2014; **111**: 6804–6809.
63 Zuleta A, Vidal RL, Armentano D, Parsons G, Hetz C. AAV-mediated delivery of the transcription factor XBP1s into the striatum reduces mutant Huntingtin aggregation in a mouse model of Huntington's disease. *Biochem Biophys Res Commun* 2012; **420**: 558–563.
64 Shankar GM, Bloodgood BL, Townsend M, Walsh DM, Selkoe DJ, Sabatini BL. Natural oligomers of the Alzheimer amyloid-beta protein induce reversible synapse loss by modulating an NMDA-type glutamate receptor-dependent signaling pathway. *J Neurosci* 2007; **27**: 2866–2875.
65 Heredia L, Helguera P, de Olmos S, Kedikian G, Sola Vigo F, LaFerla F *et al.* Phosphorylation of actin-depolymerizing factor/cofilin by LIM-kinase mediates amyloid beta-induced degeneration: a potential mechanism of neuronal dystrophy in Alzheimer's disease. *J Neurosci* 2006; **26**: 6533–6542.
66 Peterson TS, Camden JM, Wang Y, Seye CI, Wood WG, Sun GY *et al.* P2Y2 nucleotide receptor-mediated responses in brain cells. *Mol Neurobiol* 2010; **41**: 356–366.

Supplementary Information accompanies the paper on the Molecular Psychiatry website (http://www.nature.com/mp)